J Nanostruct 15(2): 720-731, Spring 2025

RESEARCH PAPER

Investigations on Magnetic and Photocatalytic Properties of $CoYb_xFe_{2-x}O_4$ Nanoparticles

Fares A. Yasseen [1] *, Hajir M. Ali [2], Rafah Mohammed Thyab [3], Ahmed Ali Mohammed [4], Huda Hadi Nameh [5], Zaid H. Mahmoud [6]

[1] *Department of Physics, Faculty of Science, University of Kufa, Al-Najaf, Iraq*

[2] *Department of Biomedical Engineering, Al-Khwarizmi College of Engineering, University of Baghdad, Baghdad, Iraq*

[3] *Department of chemistry, College of science, University of Kufa, Al-Najaf, Iraq*

[4] *Dental Technology Department, College of Medical Technology, Al-farahidi University, Baghdad, Iraq*

[5] *Pharmacy of College, University of Hilla, Babylon, Iraq*

[6] *Chemistry Department, College of Sciences, University of Diyala, Iraq*

ARTICLE INFO

Article History:
Received 10 January 2025
Accepted 20 March 2025
Published 01 April 2025

Keywords:
Yb^{3+} substitution in $CoFe_2O_4$
Magnetic properties
Methyl orange
Photocatalytic activity
Sol-gel auto-combustion

ABSTRACT

Yb^{3+} substituted $CoFe_2O_4$ nanoparticles were synthesized through sol-gel auto-combustion method. Structural investigation using X-ray diffraction (XRD) patterns confirmed the good incorporation of Yb^{3+} ions into spinel phase of $CoFe_2O_4$. Room temperature dependence of magnetic behaviors on concentration of Yb^{3+} in $CoFe_2O_4$ structure was studied using vibrating sample magnetometer (VSM). Photocatalytic enhancement was achieved by exchange interaction of Yb^{3+} with crystalline structure of $CoFe_2O_4$. The photocatalytic activity of the synthesized $CoYb_xFe_{2-x}O_4$ nanoparticles was studied by degradation of methyl orange (MO) under visible light irradiation. The degradation level of MO solution approached to 91.3% after 105 min illumination over $CoYb_{0.1}Fe_{1.9}O_4$ nanoparticles. The photocatalytic reactions were conducted at different experimental conditions to investigate the influence of photocatalyst amount and pH of dye solution on the photocatalytic efficiency of the synthesized $CoYb_xFe_{2-x}O_4$ nanoparticles. The reusability potential was studied at 7 consecutive reaction cycles, which revealed the great stability of the synthesized nanoparticles. Also, the performed photocatalytic degradation in the presence of different radical scavenging agents showed that the hydroxyl radicals are the dominant oxidative species for the degradation of MO solution.

How to cite this article
Yasseen F., Ali H., Thyab R., Mohammed A., Nameh H., Mahmoud Z. Investigations on Magnetic and Photocatalytic Properties of $CoYb_xFe_{2-x}O_4$ Nanoparticles. J Nanostruct, 2025; 15(2):720-731. DOI: 10.22052/JNS.2025.02.030

INTRODUCTION

Nanomaterials with small size and high surface area exhibit attractive properties that are very different from those of bulk, therefore they have a special position in many scientific field such as engineering, pharmaceutical, aerospace, energy production, civil construction, etc. [1-3].

Spinel ferrites—as a category of interesting nanomaterials—have received tremendous attention in the scientific communities [4-6]. Spinel ferrites with the general formula of AFe_2O_4, A is a di-valent ions, are crystallized in a face centered

* *Corresponding Author Email: fares.alkufy@uokufa.edu.iq*

cubic structure that consists of tetrahedral and octahedral sites for the accommodation of A^{2+} and Fe^{3+} cations, respectively [7, 8]. Ferrites have been used for many applications such as magnetic imaging, magnetic data storage, and photocatalysis [9-12]. The properties of the ferrites can be tuned by using of various synthesis route, introducing dopant elements, modification of composition, and alteration in cation distribution in crystalline structure [7, 10, 13].

Substitution of Co^{2+} or Fe^{3+} with di- or tri-valent cations results in substantial changes in the magnetic and photocatalytic behavior of the cobalt ferrite [14, 15] . In this way, substitution of Fe^{3+} with the larger ions from rare earth elements group is of the great interest [16, 17]. Incorporation of larger ions leads to the structural distortion and internal strains that induce alteration in the magnetic, optical, and catalytic properties of the cobalt ferrite nanomaterial [18, 19].

Specifically, photocatalytic activity is one of the most promising properties of the cobalt ferrite, on which this work is focused. Photocatalytic process defines as the use of photo-induced nanomaterial for both environmental remedies and hydrogen production [20-22]. As for environmental applications, the photocatalytic process has opened up the doors for removal of the pollutants from air, water, and soil [23, 24]. It is important to have an efficient method for getting rid of the pollutants from water resources, because they are known to be a threat to human and other life form on earth. Common pollutants include toxic chemicals (such as surfactants, fertilizers, dyes, oil, and petrochemical compounds) which are being profusely discharged into the environment [25].

Seeking for more efficient photocatalyst material with fewer adverse impacts on the environment has been a major concern in the research communities [26]. Due to the chemical stability, non-toxic, and low production cost, cobalt ferrite has been recognized as a great candidate for the environmental remedy application [27]. Moreover, effective exploiting of the photocatalytic process necessitates the recovery and reuse of the photocatalyst particles. To meet this need, the magnetic properties of the ferrite compounds provide the magnetically separation of the photocatalyst particles from the media [28-30]. For example, Vani and co-workers studied the photocatalytic activity of the Tb^{3+} substitution in cobalt ferrite for degradation of crystal violet [31]. Toloman et al. synthesized Ni substitution of $CoFe_2O_4$ nanoparticles and studied their photocatalytic activity for visible light degradation of Rhodamine B [32].

Herein, Yb^{3+} substitution in $CoFe_2O_4$ ($CoYb_xFe_{2-x}O_4$) nanoparticles have been synthesized through sol-gel auto-combustion method. Investigation of the magnetic properties of the synthesized nanoparticles was carried out by VSM analysis. The photocatalytic activity of the nanoparticles was studied for the visible light degradation of methyl orange (MO) solution.

MATERIALS AND METHODS

Synthesis of $CoYb_xFe_{2-x}O_4$ nanoparticles

The simple and straightforward sol-gel auto-combustion reaction was used to synthesize of Yb^{3+} substitution in B-site of the cobalt ferrite nanoparticles ($CoYb_xFe_{2-x}O_4$). For this purpose, first given amount of citric acid was dissolved into 50 mL of deionized water as a complexing agent. The amount of citric acid was determined to be in oxygen balance with the metal nitrate precursors. Then, different amount of nitrate precursors, that is $Co(NO_3)_2.6H_2O$, $Yb(NO_3)_3.5H_2O$, and $Fe(NO_3)_3.9H_2O$, were added to the aqueous solution of citric acid. The obtained solution was heated to 180 °C under vigorous stirring until evaporation of the water to form a dark brown viscous solution. The heating was continued to ignite the viscous solution. Finally, the solid was collected and calcined at 500 °C for 4 hours. The different molar ratio of nitrate precursors (Co:Yb:Fe) were used, as follows: 1:0:2 (x = 0), 1:0.1:1.9 (x = 0.1), and 1:0.2:1.8 (x = 0.2). According to the synthetic purpose, CFO, 0.1-CYFO, and 0.2-CYFO samples stand for the $CoFe_2O_4$, $CoYb0.1Fe_{1.9}O_4$, and $CoYb_{0.2}Fe_{1.8}O_4$ nanoparticles, respectively.

Characterization

The phase structure and crystallinity of the synthesized nanoparticles were determined using X-ray diffraction (XRD) patterns in Philips Pro PMD XRD diffractometer (Cu Kα, λ= 1.54 Å).. The morphology of the prepared nanoparticles was studied using field emission scanning electron microscope (FESEM) in TESCAN Mira3 equipped with a detector for microanalysis of the samples by energy dispersive X-ray spectroscopy (EDX). The optical properties of the nanoparticles were studied by diffuse reflectance UV-Vis spectroscopy (DRS) using JASCO UV/Vis/NIR V-670

spectrophotometer. The magnetic properties of the Yb^{3+} substituted $CoFe_2O_4$ nanoparticles was investigated at the room temperature using vibrating sample magnetometer analysis by BHV-55 VSM.

Photocatalytic activity

The photocatalytic activity of the different synthesized $CoYb_xFe_{2-x}O_4$ nanoparticles was studied using degradation of methyl orange (MO) dye under visible light irradiation. All the photocatalytic reactions were done at the same irradiation time (105 min) and concentration of MO solution (50 mL of 50 $mg.L^{-1}$). An ordinary white color LED lamp (50 W) was used as a source of the visible light, and the distance between the light source and the container of the MO solution was kept constant at 30 cm. The MO solution was allowed to reach the adsorption/desorption equilibrium with the nanoparticles under 15 min of stirring in the darkness. Then, the illuminating step was started for 105 min, and every 15 min a given amount of the MO solution (5 mL) was collected to evaluate the level of the photocatalytic degradation. The photocatalyst nanoparticles were separated from the dye solution using bar magnet. The efficiency of the visible light degradation was obtained using UV-Vis spectroscopy at maximum wavelength of MO solution (λ_{max}=465 nm).

In addition, the effect of various parameters on the level of the MO degradation was studied, including: the effect of different amount of the loaded photocatalyst, pH of MO solution, and radical scavenging agents.

RESULTS AND DISCUSSION

Structure and crystalline phase

The XRD patterns represent the crystalline structure for the different concentration of Yb^{3+} incorporated into the network of $CoFe_2O_4$ nanoparticles, shown in Fig. 1. As can be seen, the diffraction planes are corresponded to the cubic phase of the spinel of cobalt ferrite (JCPDS file no. 001-1121). There is no extra peak, which reveals that the Yb^{3+} ions are well incorporated into the $CoFe_2O_4$ structure. Due to the higher ionic radius of the Yb^{3+} (0.98 Å) with respect to the Fe^{3+} (0.64 Å), one can be expected that the crystallite size decreases by substituting of Yb^{3+} for Fe^{3+} in the $CoFe_2O_4$ network. Incorporation of larger ions leads to the lattice distortion and a decrement in the crystallinity rate. As an overall result, the average crystallite size decreases with increase the concentration of Yb^{3+} ions [33, 34]. For that, the Scherrer equation [35] was employed to determine the average crystallite size for the synthesized $CoYb_xFe_{2-x}O_4$ nanoparticles. As expected, the values of the calculated crystallite size show a decrease with increase the concentration of Yb^{3+} ions within the structure of the $CoFe_2O_4$. The

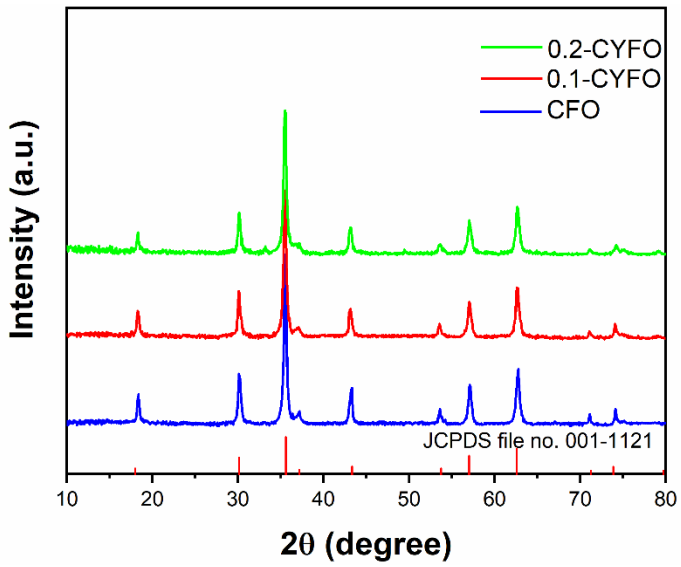

Fig. 1. XRD patterns for the $CoYb_xFe_{2-x}O_4$ nanoparticles (x = 0, 0.1, 0.2).

calculated crystallite size values for the $CoFe_2O_4$, $CoYb_{0.1}Fe_{1.9}O_4$, and $CoYb_{0.2}Fe_{1.8}O_4$ nanoparticles are 25.3 nm, 21.18 nm, and 20.68 nm, respectively.

Morphology

FESEM images for the synthesized $CoYb_xFe_{2-x}O_4$ nanoparticles are shown in Fig. 2. Clearly, the pure $CoFe_2O_4$ nanoparticles have the larger size nano-spherical particles ranging between 30-60 nm (Fig.2a). However, due to decrease of crystallite size caused by introducing of Yb^{3+}, the FESEM images (Fig.2b, c) exhibit smaller nanoparticles for the Yb^{3+} substituted CFO nanoparticles. The particle size decreased with increasing the concentration of the Yb^{3+} into the CFO structure.

EDX spectra, shown in Fig.3, represent the elemental measurements to investigate the composition of the synthesized nanoparticles

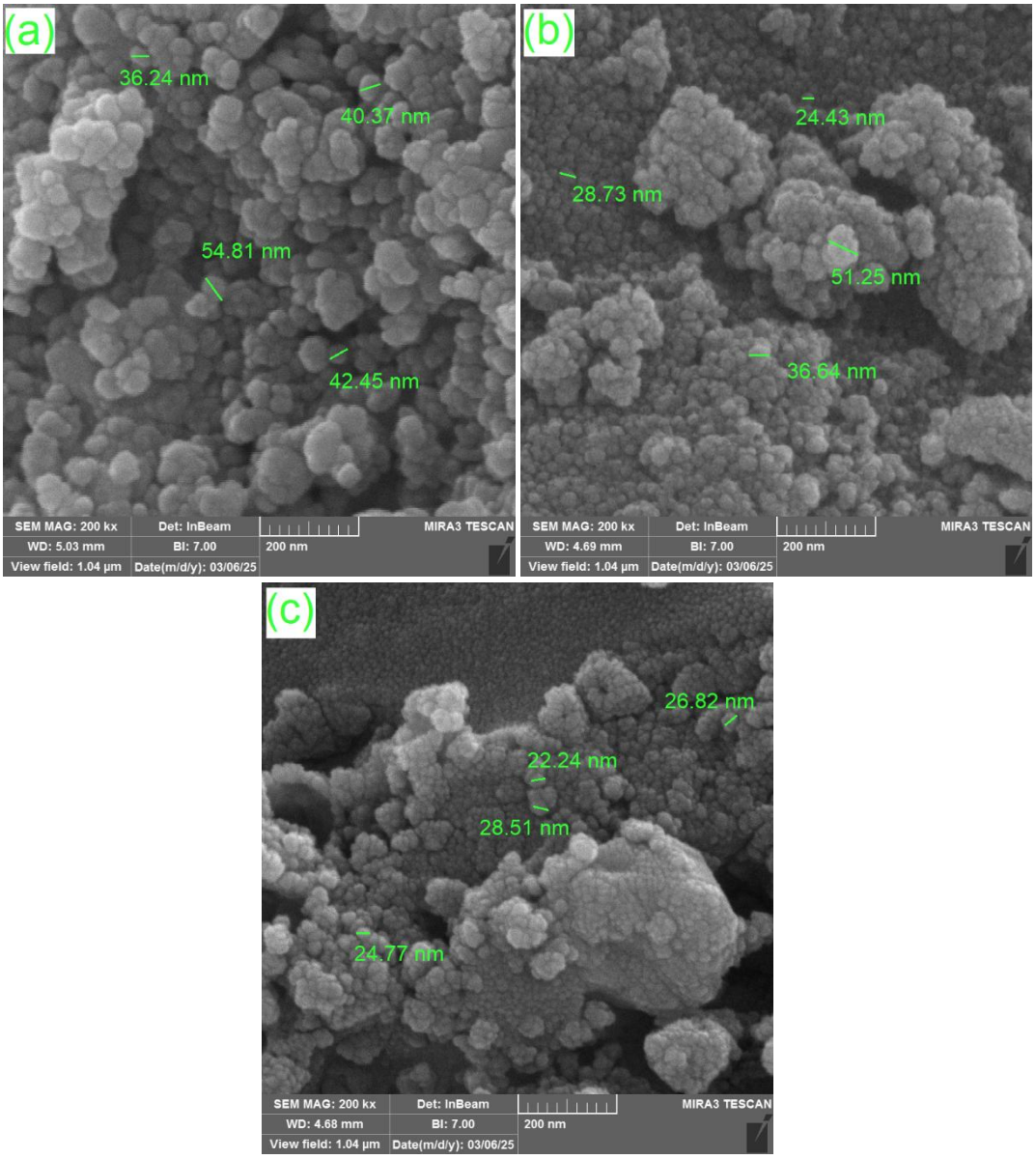

Fig. 2. FESEM images for the synthesized $CoYb_xFe_{2-x}O_4$ nanoparticles: $CoFe_2O_4$ (a), $CoYb_{0.1}Fe_{1.9}O_4$ (b), and $CoYb_{0.2}Fe_{1.8}O_4$ (c).

along with relative amount of the components. The insets to the Fig. 3 shows the amount (wt%) of each constituents existed within the nanoparticles.

Magnetic properties

The room temperature magnetization of the different synthesized $CoYb_xFe_{2-x}O_4$ nanoparticles was studied using VSM analysis. Fig. 4 shows M-H curves for the synthesized nanoparticles containing different concentration of Yb^{3+}. All the synthesized $CoYb_xFe_{2-x}O_4$ nanoparticles exhibit ferromagnetic behavior. However, the saturation magnetization (*M*s) decreases by increasing the concentration of substituted Yb^{3+} in B-site of $CoFe_2O_4$. The highest (65.52 emu/g) and lowest (40.66 emu/g) *M*s belong to the $CoFe_2O_4$ and $CoYb_{0.2}Fe_{1.8}O_4$ nanoparticles, respectively. Given to the fact that the Yb^{3+} has the lower magnetic moment (4.5 μ_B) compared to that of Fe^{3+} (5.9 μ_B), the magnetization trends are easily justified [36]. The inset to the Fig. 2 discloses the zoom on the part of the M-H curves to represent the *H*c for the synthesized nanoparticles. The decrease in the *H*c values revealed that the magnetic order was disrupted by substituting of Yb^{3+} for Fe^{3+}. Due to the fact that the Fe^{3+} ions in the $CoFe_2O_4$ structure distribute between A and B sites, introduction of the Yb^{3+} to the B site can reduce the interaction of Fe^{3+} ions. As a result, the *H*c decreases with increasing the concentration of Yb^{3+} within the $CoFe_2O_4$ crystalline structure [37]. Also, Table 1 summarizes the obtained magnetic data for all the synthesized nanoparticles.

The magnetic moment per formula unit in Bohr magneton (μ_B) [38] was obtained using the following equation:

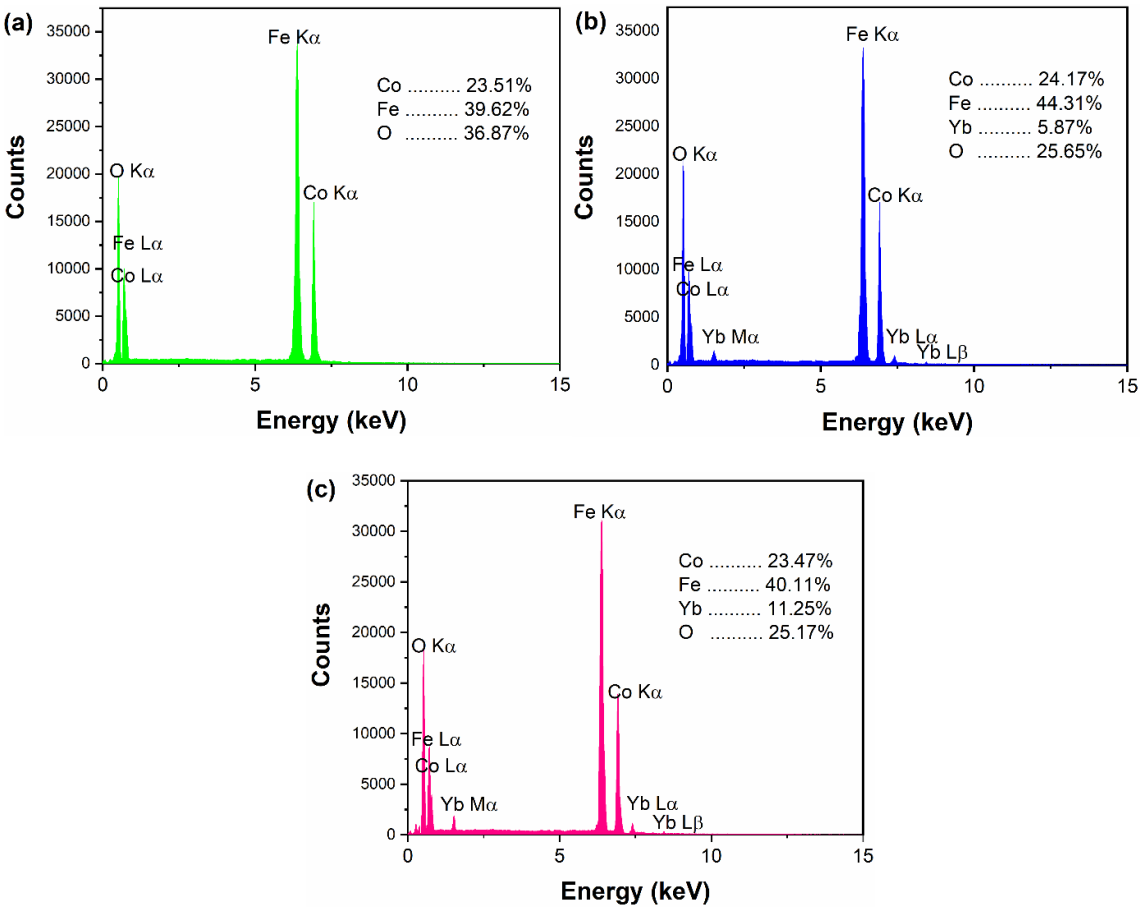

Fig. 3. EDX spectra for the synthesized $CoYb_xFe_{2-x}O_4$ nanoparticles: $CoFe_2O_4$ (a), $CoYb_{0.1}Fe_{1.9}O_4$ (b), and $CoYb_{0.2}Fe_{1.8}O_4$ (c).

$$nB = \frac{M \times Ms}{5585} \quad (1)$$

where *M* is the molecular weight of the certain composition, *M*s is the saturation magnetization.

Optical properties

The DRS spectra, shown in Fig.5, describe the optical behavior of the synthesized $CoYb_xFe_{2-x}O_4$ nanoparticles in the UV-Vis region. As seen, all the nanoparticles have the substantial absorption in the range of 400-700 nm. The absorption intensity decreased for the Yb^{3+} substituted cobalt ferrite compared to the pure $CoFe_2O_4$ nanoparticles. Also, the absorption threshold is shifted toward shorter wavelength with increasing the concentration of Yb^{3+}. This observation can be explained by dependence of absorption character on the particles size, lattice distortion and impurity centers [32, 39, 40]. According to the XRD and FESEM results, the particle size decreased with increasing the concentration of Yb^{3+} substituted for Fe^{3+} in $CoFe_2O_4$.

The band gap of the synthesized nanoparticles was calculated by Tauc method, plotting $(\alpha h\nu)^2$ versus hν and then extrapolating of the curves (Fig. 5b). The band gap values showed a blue shift associated with increasing concentration of Yb^{3+}, which is attributed to the reduced particle size [32]. The band gap values for $CoFe_2O_4$, $CoYb_{0.1}Fe_{1.9}O_4$, and $CoYb_{0.2}Fe_{1.8}O_4$ are 1.4 eV, 1.71 eV, and 2.07 eV, respectively

Photocatalytic activity

The photoactivity of the synthesized $CoYb_xFe_{2-x}O_4$ nanoparticles was studied for the degradation of MO solution under visible light irradiation. Fig.

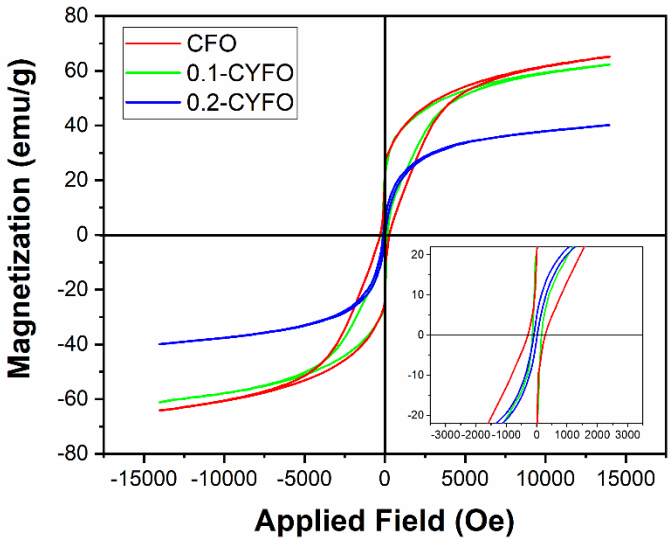

Fig. 4. Room temperature M-H plots for the different concentration of Yb^{3+} incorporated within the $CoFe_2O_4$ structure.

Table 1. Magnetic data for the synthesized $CoYb_xFe_{2-x}O_4$ nanoparticles.

Samples	$CoFe_2O_4$	$CoYb_{0.1}Fe_{1.9}O_4$	$CoYb_{0.2}Fe_{1.8}O_4$
Saturation magnetization (emu/g)	65.52	62.74	40.66
Coercivity (Oe)	315.23	155.62	51.86
Remnant magnetization (emu/g)	25.31	17.34	5.61
Residual magnetization ratio	0.386	0.276	0.137
Magnetic moment (μ_B)	2.75	2.66	1.82

6a shows that the photocatalytic efficiency of the synthesized nanoparticles is of the following order: 0.1-CYFO > 0.2-CYFO > CFO, confirming the superior photocatalytic efficiency of the $CoYb_{0.1}Fe_{1.9}O_4$ nanoparticles compared to the other synthesized nanoparticles. This result is attributed to the reduced recombination rate of the electrons/holes caused by substitution of the Yb^{3+} ions. However, more amount of Yb^{3+} induced the rapid recombination of charges, which is due to the repeated trapping of the charges [31]. These result also are in accordance with the DRS analysis, which showed the lower band gap value for the pure $CoFe_2O_4$. The narrower band gap increases the recombination of the electrons and holes [31, 41]. By visible light illuminating for 105 min, the 91.7% of the MO was degraded using 0.1-CYFO nanoparticles, whereas the pure CFO provided the MO degradation by 54.7%.

The kinetics of the photocatalytic reaction for all the synthesized nanoparticles is shown in Fig. 6b, revealing the first order kinetic rate for the nanoparticles— that is, $-\ln(C/C_0) = kt$ where k (min^{-1}) is rate constant, t (min) is the irradiation

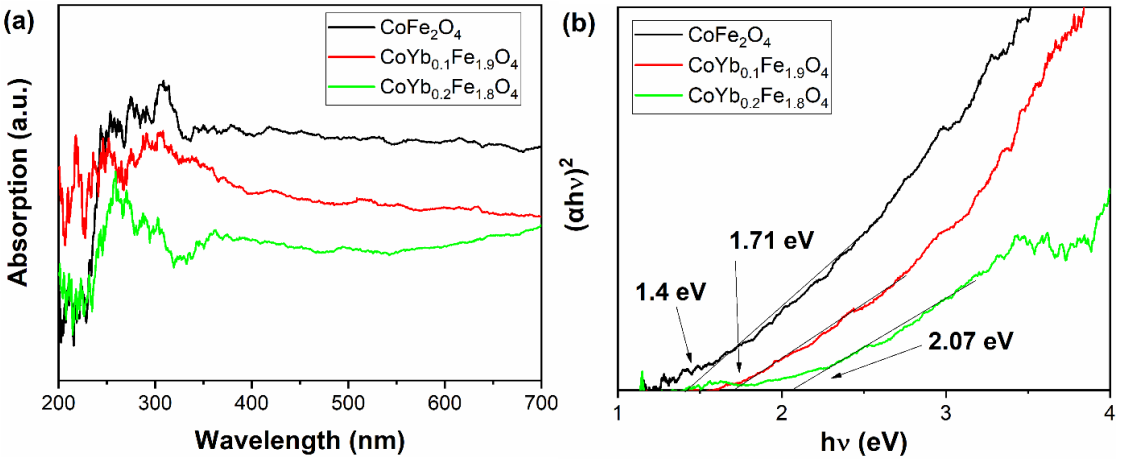

Fig. 5. DRS spectra (a) and Tauc plots (b) for the synthesized $CoYb_xFe_{2-x}O_4$ nanoparticles.

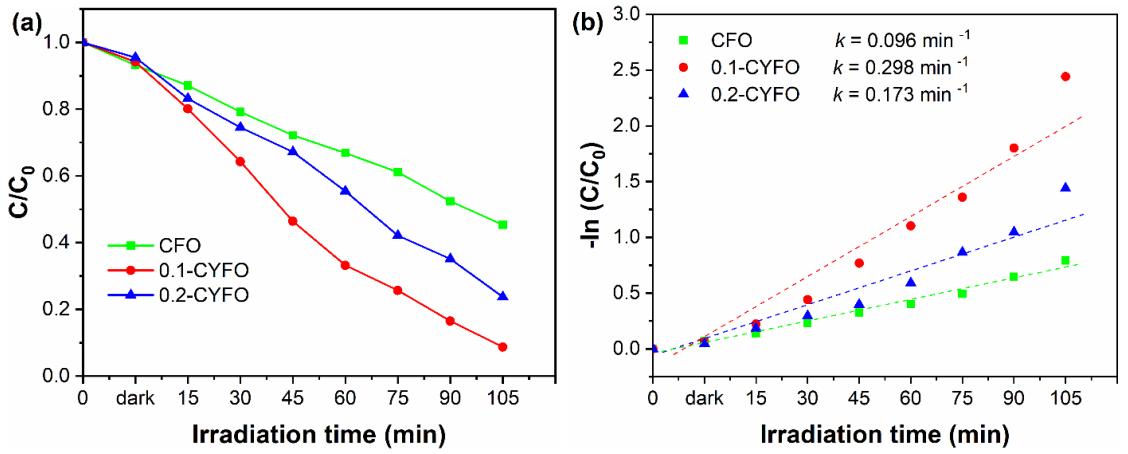

Fig. 6. Photocatalytic degradation of MO (a) and kinetic of degradation reaction (b) using different synthesized $CoYb_xFe_{2-x}O_4$ nanoparticles.

time, C, and C_0 are the concentration of dye before and after the performing the photocatalytic reaction. By plotting $-\ln(C/C_0)$ versus irradiation time, the rate constant of the reaction using the nanoparticles was calculated from the slop of the curve. The 0.1-CYFO nanoparticles indicated the highest constant rate of 0.298 min^{-1}. The other samples including 0.2-CYFO and CFO have the kinetic rate of 0.173 min^{-1} and 0.096 min^{-1}, respectively.

Also, Fig. 7 exhibits the absorption spectra of the MO solution exposed to the photocatalytic degradation using $CoYb_{0.1}Fe_{1.9}O_4$ nanoparticle at the different irradiation time. Evidently, the absorption of MO solution decreased with proceeding of the photocatalytic reaction.

Effect of dosage of photocatalyst

The photocatalytic degradation of MO solution was carried out using the different dosage of the

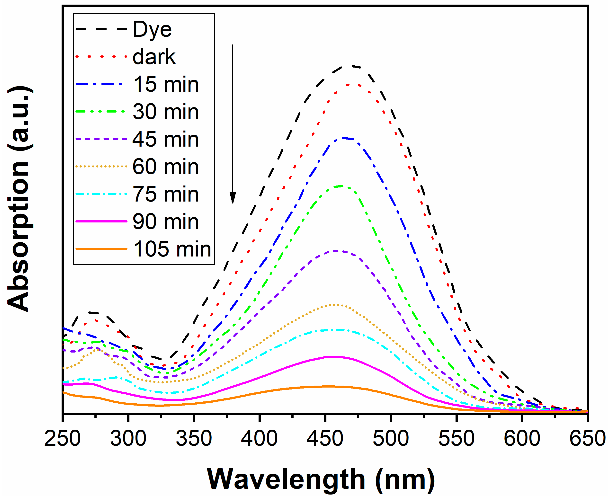

Fig. 7. UV-Vis absorption spectra for the MO solution in different irradiation time over 0.1-CLFO nanoparticles.

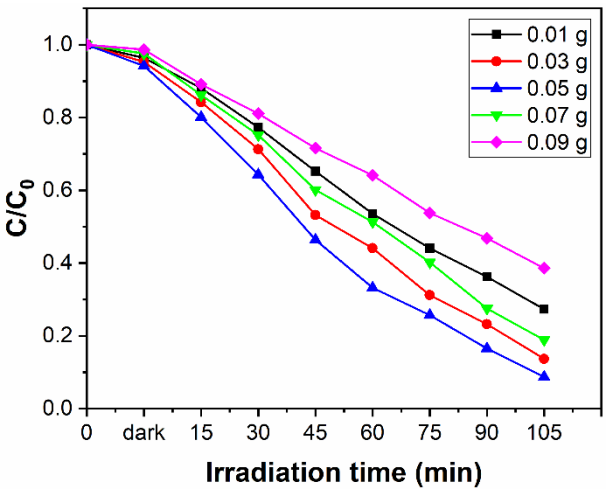

Fig. 8. Photocatalytic degradation of the MO solution using the different amount of the 0.1-CYFO nanoparticles.

0.1-CYFO nanoparticles (0.01, 0.03, 0.05, 0.07, and 0.09 g), as shown in Fig. 8.

The photodegradation of MO solution increased with increasing the amount of the photocatalyst. The highest photoactivity was obtained by using 0.05 g of the 0.1-CYFO nanoparticles. As can be seen from the Fig. 8, further amount of the nanoparticles caused to the dramatic decrement in the photodegradation level of the MO solution. This result is attributed to the limitation of the light beam to penetrate onto the turbid dye solution caused by dispersion of exceeded amount of photocatalyst nanoparticles [42].

Effect of pH

The photocatalytic efficiency of the 0.1-CYFO nanoparticles was studied at different pH of the MO solution. Due to the fact that the MO is

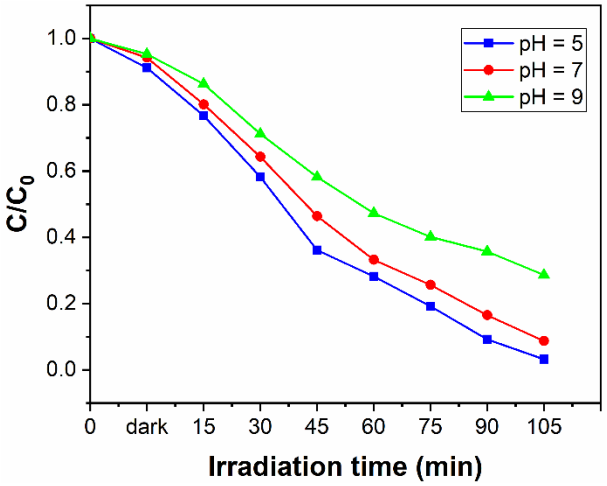

Fig. 9. Photocatalytic efficiency of the 0.1-CYFO nanoparticles at different pH values of MO solution.

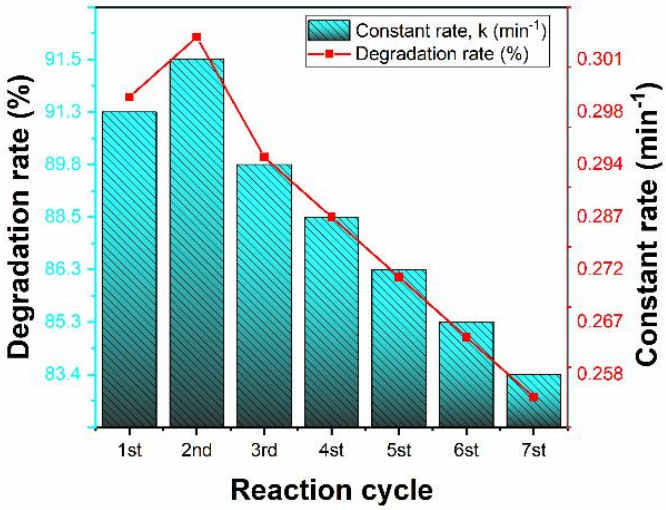

Fig. 10. Reusability of the synthesized 0.1-CYFO nanoparticles in 7 successive reaction cycles.

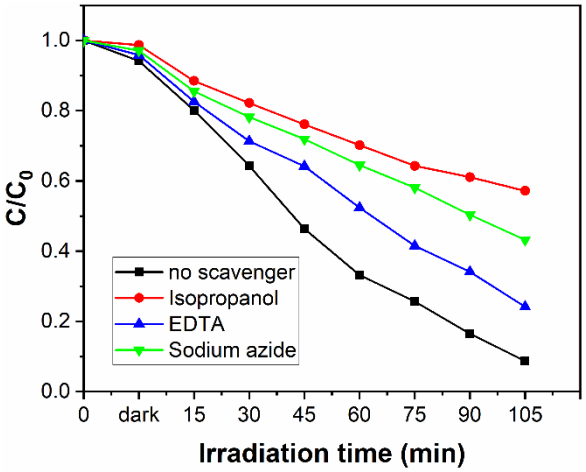

Fig. 11. Photocatalytic degradation of the MO solution in the presence of different radical scavenging agents.

an anionic dye, the positively charged surface of the photocatalyst nanoparticles is in a favor of the adsorption of the dye molecules on the photocatalyst surface [43]. Therefore, one can be expected that under acidic conditions, the degradation efficiency of the MO is higher than that of in alkaline media.

Fig.9 shows the pH dependence of the photodegradation degradation of the MO solution. As can be seen, there is an enhancement in the photocatalytic degradation level of the MO solution under acidic condition. At pH of 5, the photodegradation of the MO solution approached to more than 95%. However, an increase in the pH of MO solution to 9 resulted in a significant decrease in the photocatalytic efficiency.

Reusability studies

The photocatalytic stability of the synthesized 0.1-CYFO nanoparticles was studied at 7 consecutive reaction cycles. After each reaction, the photocatalyst was collected using a bar magnet and washed several times by deionized water/ethanol solution to remove the residual adsorbed dye. Then, the photocatalyst was heated at 100 C for 1 hour.

Fig.10 represents that the synthesized 0.1-CYFO nanoparticles have a great photocatalytic stability. The decrement of the photocatalytic efficiency is only 7.9% after 7 successive reaction cycles. Also, it can be noted that the loss of the photodegradation efficiency is not negligible after forth reaction. In addition, the variations of the constant rate of the photocatalytic reactions at 7 reaction cycles are depicted in Fig.10. The constant rate of the photocatalytic degradation using 0.1-CYFO decreased by 13% after 7 successive reaction cycles.

Mechanism of photocatalytic degradation

The photocatalytic degradation of MO solution was studied in the presence of different radical scavenging agents to find the mechanism of photocatalytic degradation over the 0.1-CYFO nanoparticles. In this case, isopropanol [44], EDTA [45], and sodium azide [45] were used as scavenging agents for quenching of the hydroxyl radicals, photo-generated holes, and superoxide radicals, respectively. Fig. 11 shows that the photocatalytic degradation of MO solution is decreased using isopropanol and sodium azide, revealing that the dominant oxidative species formed by light induced of the 0.1-CYFO nanoparticles are hydroxyl and superoxide radicals.

CONCLUSION

To sum up, we have synthesized Yb^{3+} substituted $CoFe_2O_4$ nanoparticles using simple and facile sol-gel auto-combustion method. Different concentration of Yb^{3+} ions was incorporated into the crystalline structure of the $CoFe_2O_4$ nanoparticles, and the effect of the Yb^{3+} substitution for Fe^{3+}

on magnetic and photocatalytic behavior of the $CoFe_2O_4$ was investigated. The *M*s and *H*c values were decreased by incorporation of Yb^{3+}, which is due the lower magnetic moment of the Yb^{3+} ions. However, the photocatalytic activity was benefited by the Yb^{3+} substitution, which was attributed to the contribution of Yb^{3+} in reducing the recombination rate of charge carriers. So that, the Yb^{3+} substituted $CoF_{e2}O_4$ nanoparticles disclosed the higher photocatalytic efficiency compared to the pure $CoFe_2O_4$ nanoparticles. During 105 min illumination under visible light, more than 91% of MO solution was degraded using the $CoYb_{0.1}Fe_{1.9}O_4$ nanoparticles.

CONFLICT OF INTEREST

The authors declare that there is no conflict of interests regarding the publication of this manuscript.

REFERENCES

1. Baig N, Kammakakam I, Falath W. Nanomaterials: a review of synthesis methods, properties, recent progress, and challenges. Materials Advances. 2021;2(6):1821-1871.
2. Aslam A, Razzaq A, Naz S, Amin N, Arshad MI, Nabi MAU, et al. Impact of Lanthanum-Doping on the Physical and Electrical Properties of Cobalt Ferrites. Journal of Superconductivity and Novel Magnetism. 2021;34(7):1855-1864.
3. Rahbar M, Behpour M. Fluorite type $La_2Pb_2O_7$ nanoparticles coated onto AgO as enhanced performance cathode active material for alkaline primary cell. J Power Sources. 2022;521:230887.
4. Wang L, Li S, Li J, Liu M, Xu S, Li H. Sol–gel synthesis and characterization of single-phase $CoLa_xFe_{2-x}O_4$ ferrite nanoparticles dispersed in a SiO_2 matrix. RSC Advances. 2016;6(15):12497-12503.
5. Jauhar S, Kaur J, Goyal A, Singhal S. Tuning the properties of cobalt ferrite: a road towards diverse applications. RSC Advances. 2016;6(100):97694-97719.
6. Vinosha PA, Manikandan A, Preetha AC, Dinesh A, Slimani Y, Almessiere MA, et al. Review on Recent Advances of Synthesis, Magnetic Properties, and Water Treatment Applications of Cobalt Ferrite Nanoparticles and Nanocomposites. Journal of Superconductivity and Novel Magnetism. 2021;34(4):995-1018.
7. Sharifianjazi F, Moradi M, Parvin N, Nemati A, Jafari Rad A, Sheysi N, et al. Magnetic $CoFe_2O_4$ nanoparticles doped with metal ions: A review. Ceram Int. 2020;46(11):18391-18412.
8. Humbe AV, Kounsalye JS, Shisode MV, Jadhav KM. Rietveld refinement, morphology and superparamagnetism of nanocrystalline $Ni_{0.70-x}Cu_xZn_{0.30}Fe_2O_4$ spinel ferrite. Ceram Int. 2018;44(5):5466-5472.
9. Tahar LB, Artus M, Ammar S, Smiri LS, Herbst F, Vaulay MJ, et al. Magnetic properties of $CoFe_{1.9}RE_{0.1}O_4$ nanoparticles (RE=La, Ce, Nd, Sm, Eu, Gd, Tb, Ho) prepared in polyol. J Magn Magn Mater. 2008;320(23):3242-3250.
10. Jasrotia R, Prakash J, Saddeek YB, Alluhayb AH, Younis AM, Lakshmaiya N, et al. Cobalt ferrites: Structural insights with potential applications in magnetics, dielectrics, and Catalysis. Coord Chem Rev. 2025;522:216198.
11. Salem F, Abdullah W, Noor Azman NZ. Green synthesis of manganese ferrite nanoparticles: A sustainable pathway for wastewater treatment and beyond. Journal of Water Process Engineering. 2025;71:107329.
12. Mehere AC, Jadhav VR, Kasabe SM, Rathod SM. Ni^{2+} doped cobalt nano-ferrite for gas sensing application. Results in Surfaces and Interfaces. 2025;18:100461.
13. Masunga N, Mmelesi OK, Kefeni KK, Mamba BB. Recent advances in copper ferrite nanoparticles and nanocomposites synthesis, magnetic properties and application in water treatment: Review. Journal of Environmental Chemical Engineering. 2019;7(3):103179.
14. Routray KL, Sanyal D, Behera D. Gamma irradiation induced structural, electrical, magnetic and ferroelectric transformation in bismuth doped nanosized cobalt ferrite for various applications. Mater Res Bull. 2019;110:126-134.
15. Abbas N, Rubab N, Kim K-H, Chaudhry R, Manzoor S, Raza N, et al. The photocatalytic performance and structural characteristics of nickel cobalt ferrite nanocomposites after doping with bismuth. Journal of Colloid and Interface Science. 2021;594:902-913.
16. Vani K, Hashim M, Rana G, Ismail MM, Batoo KM, Hadi M, et al. Impact of rare earth Tb^{3+} substitution in cobalt ferrites: Tuning structural, dielectric, magnetic properties and photocatalytic activity. Ceram Int. 2025;51(1):240-251.
17. Ünal B, Baykal A, Almessiere MA, Mihmanlı A. Influence of temperature and selenium substitution on electrical and dielectric characteristics of $CoFe_2O_4$ nanoparticles. J Indian Chem Soc. 2025;102(4):101620.
18. Kumar L, Kar M. Effect of La3+ substitution on the structural and magnetocrystalline anisotropy of nanocrystalline cobalt ferrite ($CoFe_2$−La O_4). Ceram Int. 2012;38(6):4771-4782.
19. Dippong T, Cadar O, Deac IG, Petean I, Levei EA, Simedru D. Influence of La^{3+} substitution on the structure, morphology and magnetic properties of $CoLa_xFe_{2-x}O_4@SiO_2$ nanocomposites. J Alloys Compd. 2024;976:172998.
20. Du J, Ahmad I, Ashraf IM, Ahmed FBM, Aslam A, Ali I, et al. Advancements in dual S-scheme heterojunction systems for photocatalytic applications: A mini-review. Int J Hydrogen Energy. 2025;100:1361-1384.
21. Khan AA, Tahir M, Khan N. Layered double hydroxide for photocatalytic application toward CO_2 reduction and water splitting: Recent advances, synthesis, heterojunction formation, challenges, and future directions. Applied Physics Reviews. 2025;12(1).
22. Geldasa FT, Dejene FB, Kebede MA, Hone FG, Jira ET. Density functional theory study of Chlorine, Fluorine, Nitrogen, and Sulfur doped rutile TiO_2 for photocatalytic application. Sci Rep. 2025;15(1):3390-3390.
23. Abed SH, Shamkhi AF, Heydaryan K, Mohammadalizadeh M, Sajadi SM. Sol-gel Pechini preparation of $CuEr_2TiO_6$ nanoparticles as highly efficient photocatalyst for visible light degradation of acid red 88. Ceram Int. 2024;50(13):24096-24102.
24. Nannou C, Maroulas KN, Tsamtzidou C, Ladomenou K, Kyzas GZ. Photocatalytic degradation of veterinary antibiotics in wastewaters: A review. Sci Total Environ. 2025;966:178765.
25. Mousavi SM, Mohtaram MS, Rasouli K, Mohtaram S, Rajabi H, Sabbaghi S. Efficient visible-light-driven photocatalytic degradation of antibiotics in water by MXene-derived TiO_2-supported SiO_2/Ti_3C_2 composites: Optimisation, mechanism and toxicity evaluation. Environ Pollut. 2025;367:125624.

26. He J, Cheng J, Lo IMC. Green photocatalytic disinfection of real sewage: efficiency evaluation and toxicity assessment of eco-friendly TiO_2-based magnetic photocatalyst under solar light. Water Res. 2021;190:116705.
27. Mmelesi OK, Masunga N, Kuvarega A, Nkambule TTI, Mamba BB, Kefeni KK. Cobalt ferrite nanoparticles and nanocomposites: Photocatalytic, antimicrobial activity and toxicity in water treatment. Mater Sci Semicond Process. 2021;123:105523.
28. Shao Z, Zeng T, He Y, Zhang D, Pu X. A novel magnetically separable $CoFe_2O_4/Cd_{0.9}Zn_{0.1}S$ photocatalyst with remarkably enhanced H_2 evolution activity under visible light irradiation. Chem Eng J. 2019;359:485-495.
29. Patil RP, Teli SB, Jadhav VD, Kamble PD, Garadkar KM. Magnetically separable $NiFe_2O_4$ nanoparticles: synthesis and photocatalytic activity. Journal of Materials Science: Materials in Electronics. 2024;35(1).
30. Bahiraei H, Azarakhsh S, Ghasemi S. Ternary $CoFe_2O_4$/g-C_3N_4/ZnO heterostructure as an efficient and magnetically separable visible-light photocatalyst: Characterization, dye purification, and mechanism. Ceram Int. 2023;49(12):21050-21059.
31. Vani K, hashim M, Ismail MM, Batoo KM, Hadi M, Kumar NP, et al. Influence of Tb^{3+} Substitution on the Structural, Optical, and Dielectric Properties of Cobalt Ferrites with Thermoelectric Assessment. Elsevier BV; 2024. http://dx.doi.org/10.2139/ssrn.4952119
32. Toloman D, Stefan M, Himcinschi C, Ganea I, Barbu L, Rostas A, et al. Impact of nickel substitution on supercapacitor and photocatalytic performances of cobalt-ferrites nanoparticles. Ceram Int. 2025;51(13):17728-17743.
33. Sharada G, Thirupathi G, Shwetha G, Kumar NP, Sowjanya P, Sreenivasu D. Synthesis, Spectral, and Magnetic Studies of Yb-Doped $CoFe_2O_4$. ECS Journal of Solid State Science and Technology. 2023;12(6):063006.
34. Sharma R, Bansal S, Singhal S. Augmenting the catalytic activity of $CoFe_2O_4$ by substituting rare earth cations into the spinel structure. RSC Advances. 2016;6(75):71676-71691.
35. Holder CF, Schaak RE. Tutorial on Powder X-ray Diffraction for Characterizing Nanoscale Materials. ACS Nano. 2019;13(7):7359-7365.
36. Jahan N, Uddin MM, Khan MNI, Chowdhury FUZ, Hasan MR, Das HN, et al. Impact of particle size on the magnetic properties of highly crystalline Yb^{3+} substituted Ni–Zn nanoferrites. Journal of Materials Science: Materials in Electronics. 2021;32(12):16528-16543.
37. Keswani BC, Patil SI, Kolekar YD, Ramana CV. Improved magnetostrictive properties of cobalt ferrite ($CoFe_2O_4$) by Mn and Dy co-substitution for magneto-mechanical sensors. J Appl Phys. 2019;126(17).
38. Singhal S, Chandra K. Cation distribution and magnetic properties in chromium-substituted nickel ferrites prepared using aerosol route. J Solid State Chem. 2007;180(1):296-300.
39. Akhtar K, Javed Y, Jamil Y, Muhammad F. Functionalized cobalt ferrite cubes: toxicity, interactions and mineralization into ferritin proteins. Applied Nanoscience. 2020;10(9):3659-3674.
40. Monisha P, Priyadharshini P, Gomathi SS, Pushpanathan K. Influence of Mn dopant on the crystallite size, optical and magnetic behaviour of $CoFe_2O_4$ magnetic nanoparticles. Journal of Physics and Chemistry of Solids. 2021;148:109654.
41. Singh Gp, Singh J, Chandel K, Arora S, Singh S, Singh D, et al. Synthesis and characterization of pristine CuO and Mg/CuO nanostructures for their anti-breast cancer and photocatalytic degradation applications: Experimental and DFT investigations. Materials Today Communications. 2024;40:109398.
42. Sathish Kumar PS, Sivakumar R, Anandan S, Madhavan J, Maruthamuthu P, Ashokkumar M. Photocatalytic degradation of Acid Red 88 using Au–TiO_2 nanoparticles in aqueous solutions. Water Res. 2008;42(19):4878-4884.
43. Hanafi MF, Sapawe N. Influence of pH on the photocatalytic degradation of methyl orange using nickel catalyst. Materials Today: Proceedings. 2020;31:339-341.
44. Elahifard MR, Gholami MR. Acid blue 92 photocatalytic degradation in the presence of scavengers by two types photocatalyst. Environmental Progress & Sustainable Energy. 2011;31(3):371-378.
45. Amini M, Ashrafi M, Gautam S, Chae KH. Rapid oxidative degradation of methylene blue by various metal oxides doped with vanadium. RSC Advances. 2015;5(47):37469-37475.